JGR Oceans

RESEARCH ARTICLE
10.1029/2019JC015134

Structure and Variability of the North Icelandic Jet From Two Years of Mooring Data

Jie Huang[1,2], Robert S. Pickart[2], Hedinn Valdimarsson[3], Peigen Lin[2], Michael A. Spall[2], and Fanghua Xu[1]

[1]Ministry of Education Key Laboratory for Earth System Modeling and Department of Earth System Science, Tsinghua University, Beijing, China, [2]Woods Hole Oceanographic Institution, Woods Hole, MA, USA, [3]Marine and Freshwater Research Institute, Reykjavik, Iceland

Key Points:
- Three different configurations of the flow on the Iceland slope north of Denmark Strait are identified using two years of mooring data
- The configuration where the North Icelandic Jet (NIJ) is dominant is baroclinically unstable and occurs during different times during the two years
- We seek to explain the seasonal timing when the NIJ is dominant on Iceland slope to upstream atmospheric forcing

Correspondence to:
J. Huang,
jhuang@whoi.edu

Citation:
Huang, J., Pickart, R. S., Valdimarsson, H., Lin, P., Spall, M. A., & Xu, F. (2019). Structure and variability of the North Icelandic Jet from two years of mooring data. *Journal of Geophysical Research: Oceans*, *124*. https://doi.org/10.1029/2019JC015134

Received 9 MAR 2019
Accepted 23 MAY 2019

Abstract Mooring data from September 2011 to July 2013 on the Iceland slope north of Denmark Strait are analyzed to better understand the structure and variability of the North Icelandic Jet (NIJ). Three basic configurations of the flow were identified: (1) a strong separated East Greenland Current (EGC) on the mid-Iceland slope coincident with a weak NIJ on the upper slope, (2) a merged separated EGC and NIJ, and (3) a strong NIJ located at its climatological mean position, coincident with a weak signature of the separated EGC at the base of the Iceland slope. Our study reveals that the NIJ-dominant scenario was present during different times of the year for the two successive mooring deployments—appearing mainly from September to February the first year and from January to July the second year. Furthermore, when this scenario was active it varied on short timescales. An energetics analysis demonstrates that the high-frequency variability is driven by mean-to-eddy baroclinic conversion at the shoreward edge of the NIJ, consistent with previous modeling work. The seasonal timing of the NIJ dominant scenario is investigated in relation to the atmospheric forcing upstream of Denmark Strait. The resulting lagged correlations imply that strong turbulent heat fluxes in a localized region on the continental slope of Iceland, south of the Spar Fracture zone, lead to a stronger NIJ dominant state with a two-month lag. This can be explained dynamically in terms of previous modeling work addressing the circulation response to dense water formation near an island.

Plain Language Summary The dense water flowing southward through Denmark Strait represents the largest contribution to the deep limb of the Atlantic Meridional Overturning Circulation, the large-scale flow pattern that helps regulate Earth's climate. Three different currents feed the overflow in the strait: the shelfbreak East Greenland Current adjacent to Greenland, the separated East Greenland Current located farther offshore, and the North Icelandic Jet (NIJ) on the Iceland continental slope. The latter, which was recently discovered, supplies the deepest and densest overflow water to the strait. To understand the structure and variability of the NIJ, we analyze two years of mooring data on the Iceland slope roughly 200 km northeast of Denmark strait. We present the spatial and temporal variability of three configurations of the flow and focus on the NIJ-dominant scenario. The rapid (less than 1 week) variability is found to arise from instability associated with the current's density structure. We then address the monthly variation, which we argue is driven by air-sea heat fluxes in a localized region on the continental slope north of Iceland. The ocean responds to the fluxes in this region by exciting waves that propagate clockwise around the island, which in turn impact the strength of the NIJ.

1. Introduction

The circulation in the Nordic Seas plays a critical role for the North Atlantic climate system. Warm, saline Atlantic waters flow northward, release heat to the atmosphere, and the newly ventilated dense waters sink, return southward, and enter the North Atlantic as overflow plumes. This sinking represents an important component of the Atlantic Meridional Overturning Circulation. Previous studies (Dickson & Brown, 1994; Jochumsen et al., 2017) indicate that approximately 50% of the total overflow water passes through Denmark Strait. However, there remain significant gaps in our knowledge of the upstream sources and pathways of water feeding the strait, especially with regard to the newly identified North Icelandic Jet (NIJ) (Jonsson & Valdimarsson, 2004; Pickart et al., 2017; Våge et al., 2011). This in turn hinders our ability to establish the sensitivity of the Atlantic Meridional Overturning Circulation to changes in the freshwater

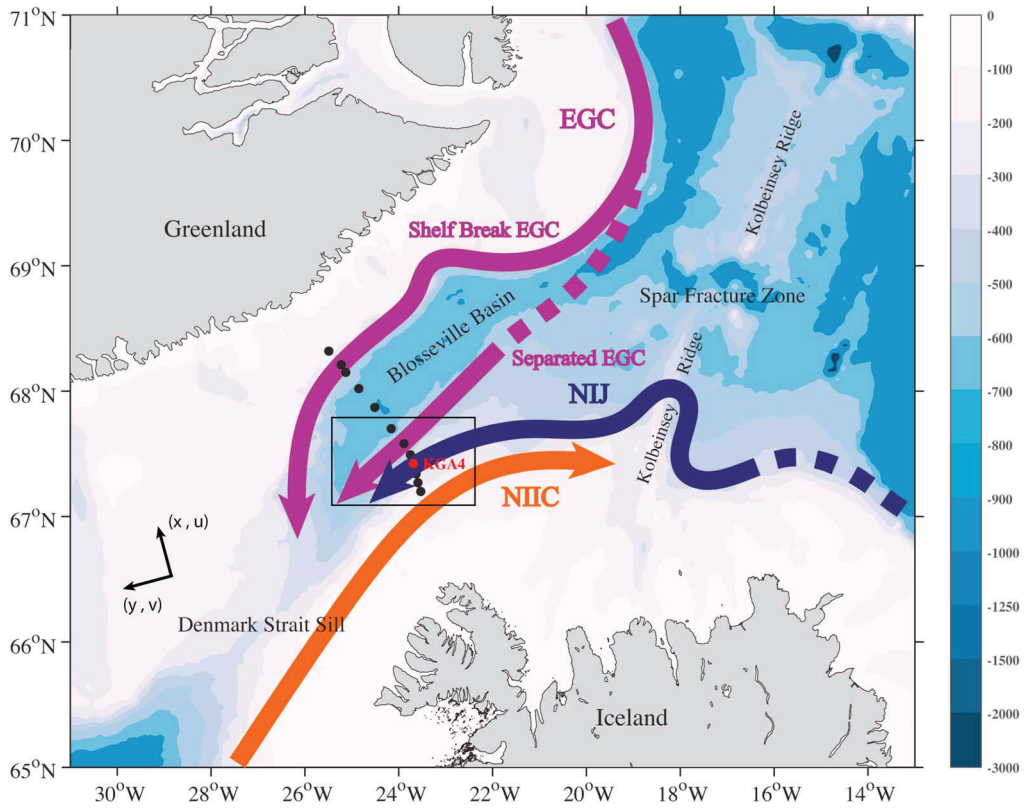

Figure 1. Schematic circulation upstream of Denmark Strait and place names. The North Icelandic Jet (NIJ), the North Icelandic Irminger Current (NIIC), and the East Greenland Current (EGC) are shown in black, orange, and purple, respectively. The EGC bifurcates in the Blosseville Basin forming the shelfbreak branch and the separated branch. The dashed portions of the arrows represent parts of the pathways that require further clarification. The black circles denote the mooring locations of the Kögur array; mooring KGA4 is highlighted as this is the only site instrumented in the second year. The bathymetry is from ETOPO2. The rotated coordinate system used in the study is indicated. The box outlines the portion of the Kögur array used in the study.

input (Dukhovskoy et al., 2016; Gierz et al., 2015), air-sea fluxes (Moore et al., 2012), and sea ice concentration (Moore et al., 2015) in the Nordic Seas.

The circulation scheme and pathways of overflow water upstream of Denmark Strait have recently been revised as a result of the discovery of the NIJ (Figure 1). Prior to this it was believed that the East Greenland Current (EGC) along the Greenland shelfbreak and slope was the sole conduit of Denmark Strait Overflow Water (DSOW) (Mauritzen, 1996). However, Jonsson and Valdimarsson (2004) reported the existence of a new current, which subsequently has been termed the NIJ, transporting the densest component of overflow water into Denmark Strait along the north slope of Iceland. Together with more recent measurements and model simulations (Behrens et al., 2017; Harden et al., 2016; Köhl et al., 2007; Våge et al., 2011; Våge et al., 2013), it has now been established that there are three distinct currents advecting overflow water southward into the strait: the shelfbreak EGC, the separated branch of the EGC, and the NIJ (Figure 1). The separated EGC bifurcates from the shelfbreak EGC as it approaches the Blosseville Basin. Two mechanisms have been proposed to explain the bifurcation (Våge et al., 2013). The first explanation is that the separated EGC results from the negative wind stress curl in the region together with the closed bathymetric contours of the Blosseville Basin. The second explanation is that the shelfbreak EGC is baroclinically unstable and the separated branch arises from the rectification of eddies spawned by the shelfbreak branch.

Using a yearlong mooring array deployed north of Denmark Strait along the so-called Kögur section (Figure 1), Harden et al. (2016) estimated the transport of overflow water by the three currents, deducing that the shelfbreak EGC accounts for 42% (1.50 Sv), the separated EGC for 30% (1.04 Sv), and the NIJ for

28% (1.00 Sv). Consistent with the transport of DSOW at the sill (Jochumsen et al., 2012; Jónsson & Valdimarsson, 2012), there is no significant seasonal cycle of the total transport of the three pathways at the Kögur line, but the transport of the NIJ is generally out of phase with the combined transports of shelfbreak EGC and separated EGC (Harden et al., 2016). As the three currents approach the sill, the NIJ merges with the separated EGC. Using historical hydrographic data in Denmark Strait and an end-member analysis, Mastropole et al. (2017) determined that the deepest part of the overflow water in the strait is associated with the NIJ water, while the water transported by shelfbreak EGC passes through the strait in the vicinity of Greenland shelfbreak. The cold, fresh water mass in the NIJ is referred to as Arctic-origin water because it is ventilated in the interior Nordic Seas. By contrast, the warm, salty water mass in the EGC is termed Atlantic-origin water as it is ventilated within the rim current flowing around the Nordic Seas and thus has a direct advective pathway stemming from the North Atlantic (Mauritzen, 1996; Pickart et al., 2017).

While the NIJ is now established as a significant source of DSOW, there remain numerous open questions with regard to its origin, path, variability, and dynamics. The source of the water in the NIJ has been discussed in several previous studies (Käse et al., 2009; Köhl, 2010; Pickart et al., 2017; Våge et al., 2011). The leading hypothesis (Våge et al., 2011) is that the NIJ originates from the Iceland Sea as the lower limb of a local overturning cell. In this scheme the North Icelandic Irminger Current (NIIC) is the upper limb of the cell, carrying warm Atlantic water northward that is transformed by wintertime air-sea interaction and returns equatorward in the NIJ. Pickart et al. (2017) found that the interannual variability in the salinity of the outflowing NIJ is in phase with the changes in evaporation minus precipitation (E−P) over the region of dense water formation, suggesting that the overturning process is rapid. This casts doubt on the Iceland Sea Gyre as the location where the densification takes place, due to the fact that the water is trapped to some degree within the gyre. The recent observations of Våge et al. (2015) indicate that the deepest and densest wintertime mixed-layers occur to the northwest of the gyre, which seemingly allows for a more direct connection to the NIJ. Aside from the origin of the dense water in the NIJ, its establishment as a current remains largely unexplained, as does its variability. Harden and Pickart (2018) identified the presence of high-frequency (order days) topographic Rossby Waves in the current, which appear to originate from the meandering of the separated EGC in the Blosseville Basin. However, it is still unclear how the NIJ behaves on longer timescales and if it is influenced by downstream processes in Denmark Strait or upstream processes in the Nordic Seas.

In this study, we analyze two years of mooring data (September 2011 to July 2013) from the Kögur section north of the Denmark Strait sill in order to shed more light on the characteristics and variability of the NIJ. Using the first year of data, when there were multiple moorings, the currents on the Iceland slope are classified into three basic configurations: (1) a strong separated EGC and weak NIJ, which are clearly distinct; (2) a merged separated EGC and NIJ; and (3) a strong NIJ and weak separated EGC, which are again distinct. We are then able to apply this classification system to the second year of data when there was only a single mooring. We begin with a presentation of the data used in the study. This is followed by an investigation of the general spatial and temporal variability of circulation on the Iceland slope, which leads to our classification of the three configurations of the flow. Next we focus on the NIJ-dominant configuration and investigate the instability and energetics of this state. Finally, we explore the relationship between the NIJ-dominant type and the atmospheric forcing.

2. Data and Methods

2.1. Mooring Data

Here we use two years of data from a set of moorings deployed along the Kögur section (approximately 200 km upstream of the Denmark Strait sill; Figure 1). In the first year (September 2011 to July 2012), there were 12 moorings spanning the section, named KGA1-12, measuring both the hydrography and velocity of the water column from 50 m to the bottom. A detailed description of the first-year mooring data, including the instrumentation, processing steps, and sensor accuracy, is presented in Harden et al. (2016). The instrumentation consisted of a combination of MicroCATs and Coastal Moored Profilers measuring pressure, temperature, and salinity, and Recording Current Meters and acoustic Doppler current profilers measuring velocity. The configuration of the moorings over the Iceland slope

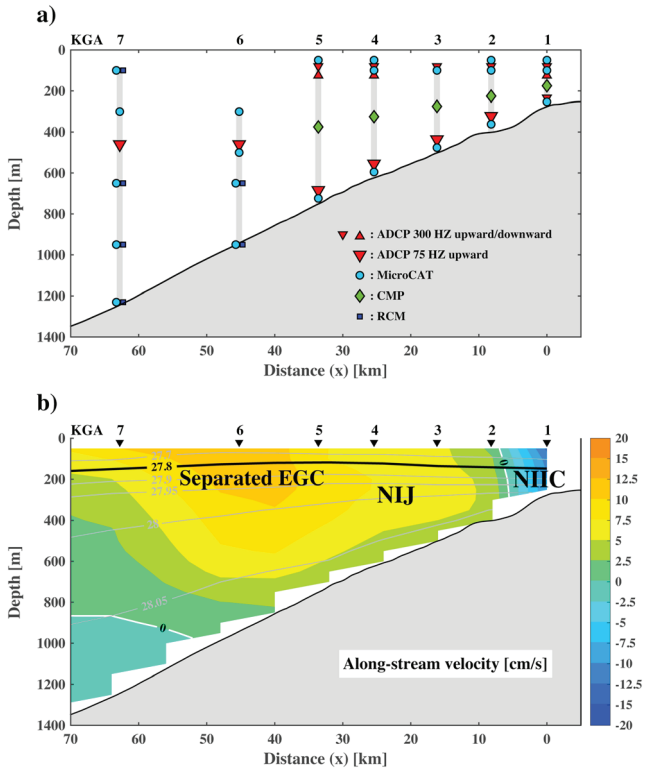

Figure 2. (a) Configuration and instrumentation of the portion of the Kögur mooring array used in the study (delineated by the box in Figure 1). The names of the moorings are listed along the top (KGA1-KGA7). The different types of instruments are marked in the legend. (b) Mean vertical section of the along-stream velocity [color, cm/s] in the first year, overlain by the mean potential density [grey contours, kg/m^3]. The zero velocity value is contoured white. The 27.8 kg/m^3 isopycnal is highlighted black, denoting the top of the dense overflow water layer.

is shown in Figure 2a. We use the gridded product constructed by Harden et al. (2016), which is an 8-hourly time series of vertical sections with a lateral resolution of 8 km and vertical resolution of 50 m. Since we are focusing on the Iceland slope, we only consider the southeastern part of the mooring array (moorings KGA1-7, delimited by the black box in Figure 1 and situated approximately 70 km offshore of the Iceland shelfbreak). Velocities were rotated to be along-stream (v, positive direction of 255°T) and cross-stream (u, positive direction of 345°T). As discussed in Harden et al. (2016), in the yearlong mean vertical section of along-stream velocity the separated EGC is merged with the NIJ, while the seaward edge of the NIIC is present at mooring KGA-1 (Figure 2b).

In the second year, only the KGA4 mooring was redeployed on the Iceland slope (August 2012 to July 2013). The hydrographic and velocity instrumentation was the same as in the initial deployment, and the data were processed following the same procedures used for the first year.

2.2. Meteorological Data

To explore the relationship between the circulation and atmospheric forcing, we used the ERA-Interim reanalysis product from the European Center for Medium-Range Weather Forecast (ECMWF, https://www.ecmwf.int). This product has been used extensively in previous studies investigating the air-sea interaction along the coast of Greenland and in the Nordic Seas and has been shown to be accurate (Harden et al., 2011; Harden et al., 2016; Våge et al., 2015). Here we use wind, sea level pressure, sea ice concentration, and latent and sensible heat flux data, with daily temporal resolution and 0.25° spatial resolution.

2.3. Ertel Potential Vorticity

To shed light on the stability characteristics of the flow, we use the gridded vertical sections from the first year of data to calculate the Ertel potential vorticity

$$\Pi = \frac{-f}{\rho_0}\frac{\partial \sigma_\theta}{\partial z} - \frac{1}{\rho_0}\left(\frac{\partial v}{\partial x} - \frac{\partial u}{\partial y}\right)\frac{\partial \sigma_\theta}{\partial z} + \frac{1}{\rho_0}\frac{\partial v}{\partial z}\frac{\partial \sigma_\theta}{\partial x}, \quad (1)$$

where f is the (constant) Coriolis parameter (1.45×10^{-4} s^{-1}), ρ_0 is the reference density (1.028×10^3 kg/m^3) calculated using the mean mooring data, and σ_θ is the potential density. The three terms on the right-hand side of equation (1) are the planetary vertical stretching term, the relative vorticity term, and the tilting term (from left to right). The relative vorticity term is dominated by horizontal gradient of the along-stream velocity ($\frac{\partial v}{\partial x}$).

2.4. Mean-to-Eddy Conversion

The energetics of the circulation is addressed by evaluating the conversion terms from the mean energy to the eddy energy. Following Spall et al. (2008), baroclinic instability is linked to the conversion from mean potential energy into eddy energy and is given by

$$\mathrm{BC} = -\mathrm{g}\,\gamma\overline{u'\sigma'_\theta}/\rho_0, \quad (2)$$

where g is the gravitational acceleration, $\gamma = \partial z/\partial x$ is the mean isopycnal slope, and $\overline{u'\sigma'_\theta}$ is the eddy density flux. The primes indicate deviations from the time mean, and the overbar indicates the time mean. Positive values correspond to energy being transferred from the mean density field to eddy activity.

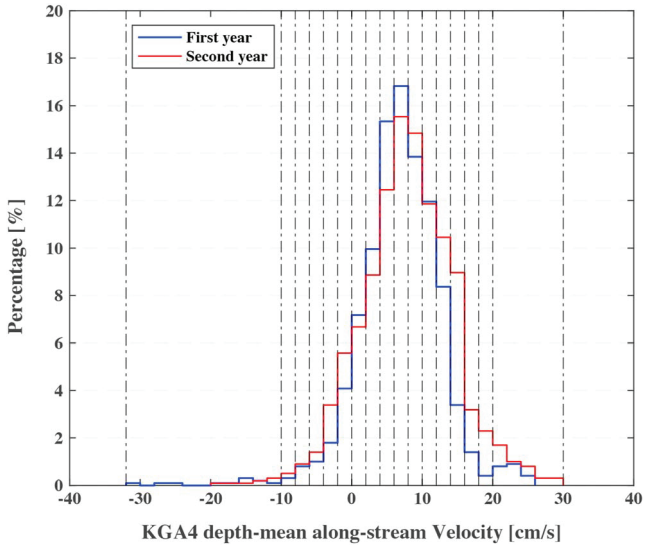

Figure 3. Histogram of the depth-mean along-stream velocity ($KGA4_{vel}$) in the first (blue) and second year (red). Positive velocity indicates equatorward flow.

Barotropic instability is related to the conversion from mean kinetic energy and is given by

$$BT = -\overline{u'v'}\,\frac{\partial \overline{v}}{\partial x}, \tag{3}$$

where $\overline{u'v'}$ is the eddy momentum flux and $\frac{\partial \overline{v}}{\partial x}$ is the cross-stream gradient of the time mean along-stream velocity. Positive values correspond to energy being transferred from the mean current to eddy activity.

3. Results

3.1. Three Current Regimes Using the First Year of Mooring Array Data

The mean vertical section of along-stream velocity in the first year (Figure 2b) reveals that the separated EGC is merged with the NIJ. The separated EGC is surface intensified and centered near mooring KGA6. Progressing onshore, the flow becomes middepth-intensified, which is characteristic of the NIJ (Våge et al., 2011). Upstream of the Kögur line, the core of the NIJ is situated near the 650-m isobath, which is consistent with the mean section in Figure 2b. At the shoreward end of the mean section the northward flowing NIIC is present.

To assess the spatial variability of the current on the Iceland slope, with an eye toward the fact that we only have the single mooring KGA4 in year two, we identified different flow regimes using the data from the KGA4 mooring as the basis for the characterization. In particular, using the first year of data, we computed the depth-mean along-stream velocity at KGA4 at each time step and separated the results into bins of 2-cm/s increments (Figure 3). One sees that, most commonly, the depth-mean flow at this site is equatorward in the range of 6-10 cm/s. The entire range in values spans from approximately -30 cm/s to +30 cm/s, although the extreme values are rare. Based on this, we constructed 17 composite mean vertical sections using all 7 moorings (the 17 bins are marked in Figure 3).

The composited along-stream velocity section for each bin is shown in Figure 4, with the range of depth-mean along-stream velocity at the KGA4 mooring (referred to as $KGA4_{vel}$) and the frequency (in percentage) of each bin listed above the section. A clear pattern of the circulation on the Iceland slope emerged as $KGA4_{vel}$ increased from negative to positive values (Figure 4). For all cases when $KGA4_{vel}$ is smaller than 4 cm/s, the separated EGC and the NIJ are distinct, with the separated EGC significantly stronger than the NIJ. In these cases, the NIJ is located roughly 0-25 km offshore of the shelfbreak (the KGA4 mooring is located at $x = 25$ km). For larger values of $KGA4_{vel}$, the separated EGC and the NIJ start to merge and become undistinguishable when $KGA4_{vel}$ ranges from 4 to 12 cm/s. This situation is similar to the year-round mean. Finally, when $KGA4_{vel}$ increases beyond 12 cm/s, the NIJ becomes dominant with a weak signature of the separated EGC at the base of the Iceland slope. Note that in this scenario the location of the NIJ shifts offshore (x=15-35 km). The subsurface velocity maximum of NIJ is centered near 250-m depth, with a core value >15 cm/s. Thus, the binned vertical sections indicate a clear evolution in the spatial structure of flow with the increase of the velocity at the KGA4 mooring. In all cases the northward flowing NIIC is present at the shoreward end of the section.

To simplify the analysis, we consider three scenarios for which we constructed composite vertical sections (Figures 5a, 5c, and 5e): (1) type1 is referred to as the strong separated EGC (corresponding to $KGA4_{vel} \leq 4$ cm/s), which has a weak signature of the NIJ at shallow depths on the Iceland slope; (2) type2 is referred to as the merged separated EGC-NIJ (corresponding to 4 cm/s < $KGA4_{vel} \leq 12$ cm/s); and (3) type3 is referred to as the dominant NIJ (corresponding to $KGA4_{vel} > 12$ cm/s), which has a weak presence of the separated EGC at the base of the Iceland slope. In this scenario, the NIJ is located at its canonical location near the 650-m isobath. The frequency of occurrence of type1, type2, and type3 is 26%, 58%, and 16%, respectively, over the first year of data.

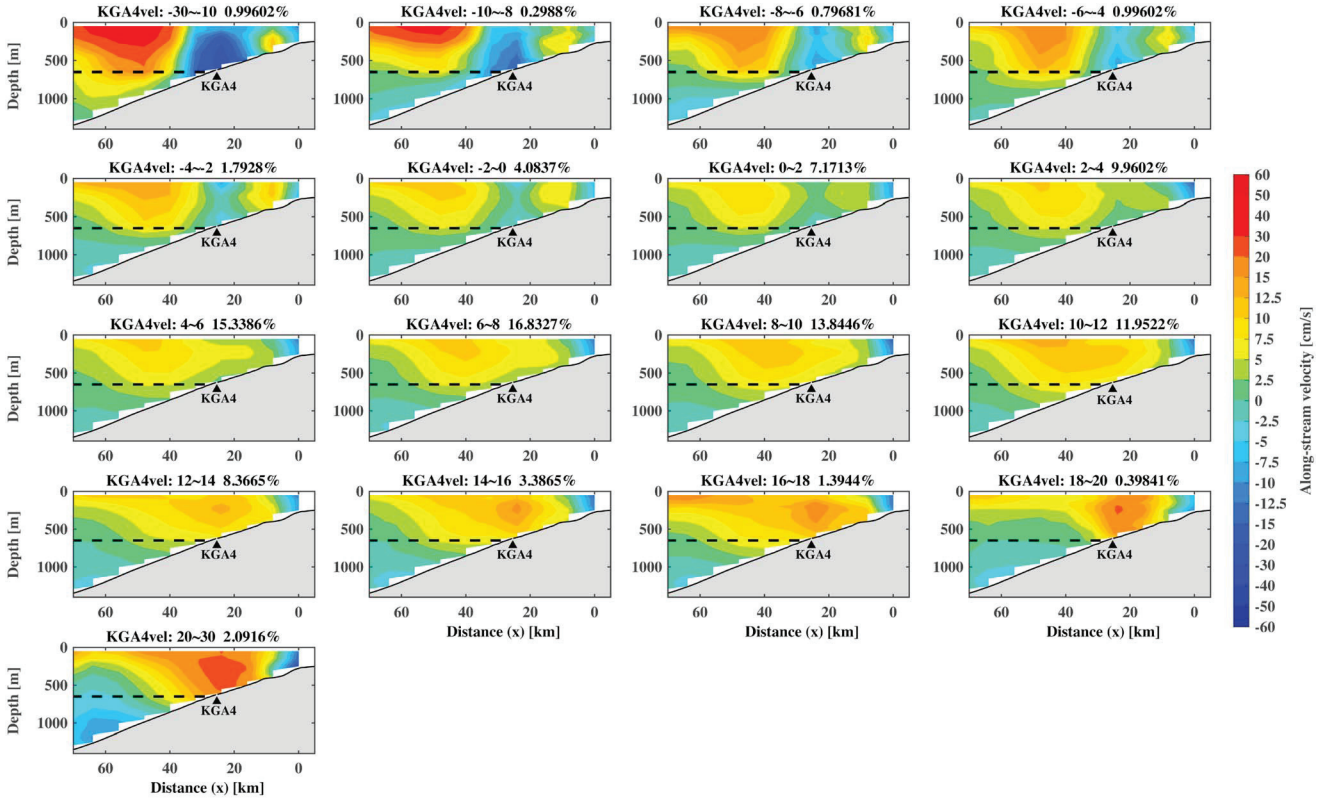

Figure 4. Composite vertical sections of along-stream velocity corresponding to the binned values of $KGA4_{vel}$ (see text for details). The value of the bin, along with the percent of the time that it is present through the year, are listed above each section. The location of the KGA4 mooring is shown by the black triangle. The horizontal dashed black line indicates the depth of the Denmark Strait sill.

The corresponding composite vertical sections of density anomaly for each type are shown in Figures 5b, 5d, and 5f. Note that for the NIJ-dominant type3, there is a positive density anomaly in the 200- to 400-m depth range at the KGA4 mooring (Figure 5f), close to the subsurface maximum velocity of the NIJ (Figure 5e). The magnitude of the density anomaly is small but statistically significant, indicating that when the NIJ is strong, it transports denser water in its core. By contrast, for type1 when the NIJ is relatively weak, it transports anomalously lighter water at its core. From hereon we focus primarily on type3 to understand the nature and dynamics of the NIJ.

3.2. Temporal Variability of the NIJ-Dominant Scenario From Two Years of Mooring Data

Using the above identified configurations, we plot the time series of $KGA4_{vel}$ for both years and identify the occurrences of each current type (Figures 6a and 6c). Focusing on year-1, the appearance of the NIJ-dominant type (red color in Figure 6a) shows a significant seasonal variation, with a greater appearance frequency from September to February. Figure 6b presents the time series of density at the KGA4 mooring averaged over 200- to 400-m depth range. The reason to focus on the density in this range is that the NIJ is centered in this layer, with a maximum in velocity and density anomaly (Figures 5e and 5f). Not surprisingly, higher values of density occur from November to March, consistent with the appearance of the NIJ-dominant type. Note that there are many pulses in the time series of velocity of type3 (Figure 6a), indicating temporal variability in the NIJ-dominant scenario on a variety of timescales from days to seasons.

In year-2 there are some notable changes. First, the yearlong mean velocity at mooring KGA4 increases, although it still displays the characteristic vertical structure of the NIJ with a middepth maximum in velocity (not shown). Using the same classification criterion (defined by $KGA4_{vel}$), the histogram of values through the year is similar (Figure 3). However, the appearance of the NIJ-dominant type appears mainly from January to July (Figure 6c), significantly different than that of the first year (Figure 6a), although it has the same pulse-like character during the time of year that it is prevalent. Consistent with year-1, the time

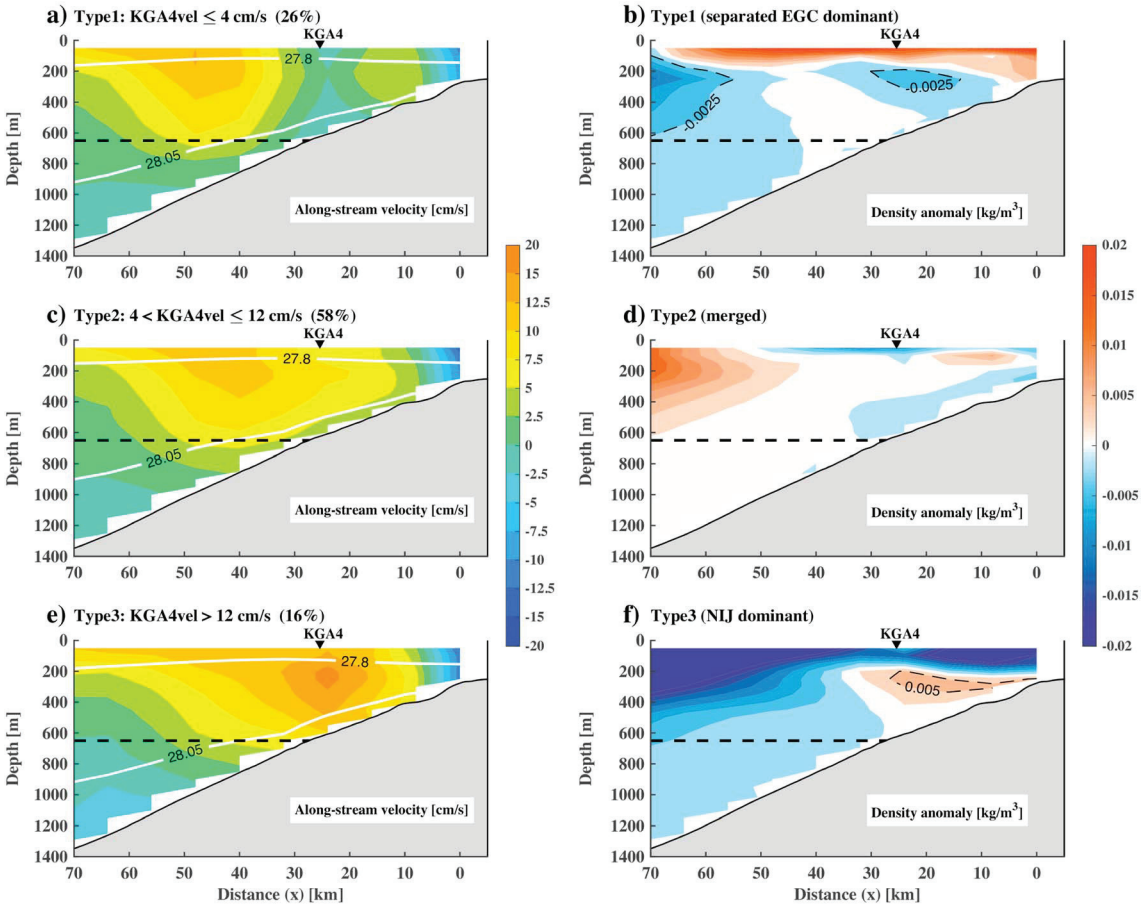

Figure 5. (a, c, and e) Composite mean sections of the along-stream velocity [color, cm/s] for the three characteristic configurations of the flow on the Iceland slope, using the first year of data. The 27.8 and 28.05 isopycnals are highlighted by the white contours. The range of $KGA4_{vel}$ values for each composite and the percent of the time that the configuration is present through the year are listed above each section. The horizontal dashed black line indicates the depth of the Denmark Strait sill. The location of KGA4 mooring is shown by the black triangle. (b, d, and f) The density anomaly, relative to the yearlong mean, for the three composites [color, kg/m^3].

series of density averaged over 200- to 400-m depth for the second year shows generally higher densities during the NIJ dominant period (Figure 6d).

Harden et al. (2016) found that even though the total transport of dense overflow water upstream of Denmark Strait—that is, the sum of the two EGC branches and the NIJ—has no significant seasonal signal, the transport of overflow water by the NIJ varied through the year. Our results imply that while there was again variation in the NIJ dominant state on the Iceland slope the following year, the seasonal trend was not consistent between the two years. It is thus of interest to investigate possible mechanisms resulting in the different appearance of the NIJ-dominant state in the two consecutive years. In addition, we seek to explore the nature of the short timescale fluctuations when this scenario is present. We consider the high-frequency variability first.

3.3. Instability and Energetics of the NIJ-Dominant Type

The potential vorticity provides a means to assess the stability characteristics of the flow. Using the first year of data, the mean vertical sections of the total Ertel potential vorticity for the time period when the separated EGC is dominant (type1) versus the time period when the NIJ is dominant (type3) are shown in Figures 7a and 7b. Both sections display similar characteristics and are dictated predominantly by the stratification (the stretching term in equation (1)). Two regions with high potential vorticity Π are found, centered at x=30 km and x=0 km (the values are higher for the type3 scenario), while the values decrease at depth. A necessary condition for baroclinic instability of the current is that the cross-stream gradient of potential vorticity, Π_x,

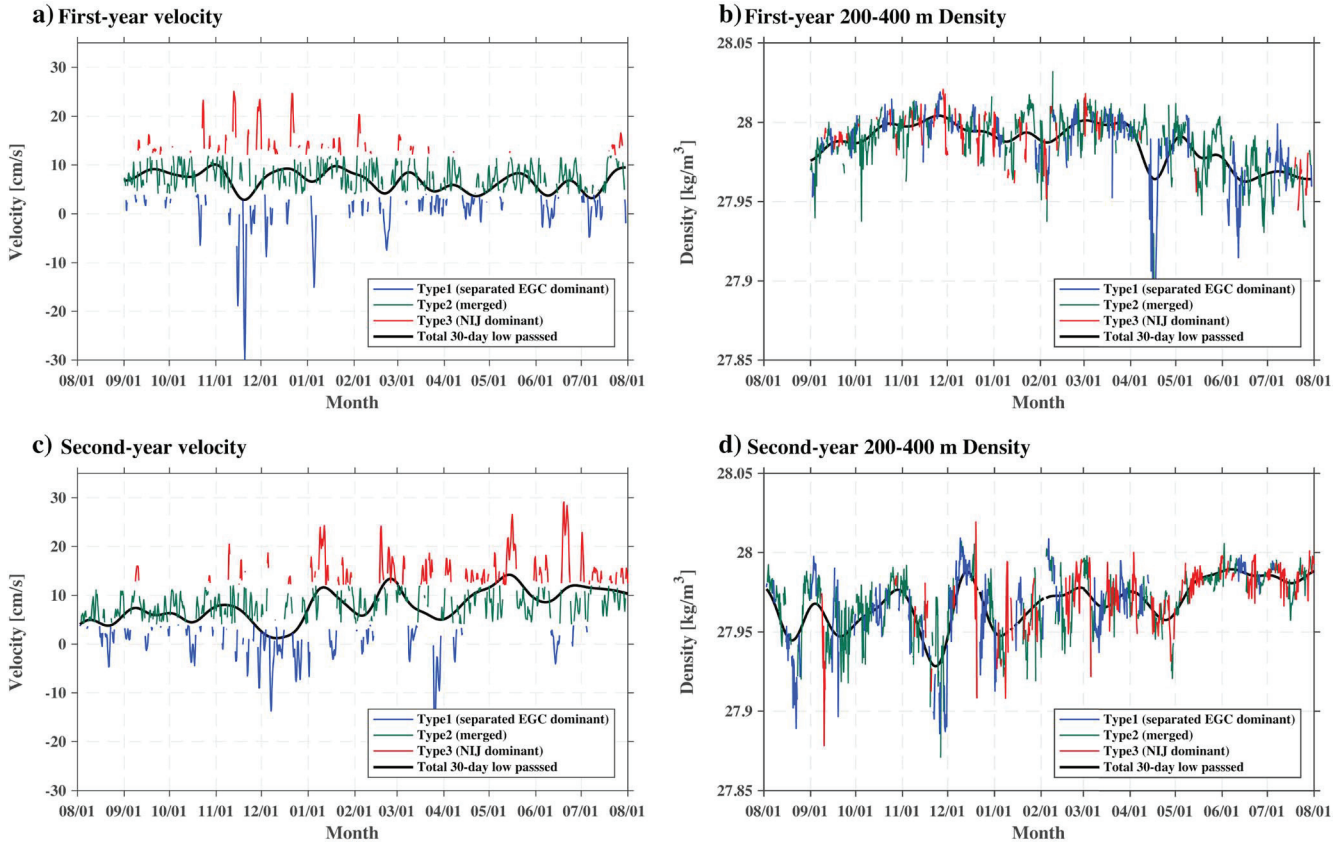

Figure 6. Time series of the depth-mean along-stream velocity ($KGA4_{vel}$) and the density averaged over 200- to 400-m depth at KGA4 in (a and b) the first year and (c and d) the second year for the three configurations of the flow on the Iceland slope (see the legend). The 30-day low-pass of the full time series are shown in black.

changes sign with depth (Charney & Stern, 1962). In Figures 7c and 7d, we present the vertical sections of Π_x for the two periods. Again, both sections are qualitatively similar and reveal that the conditions for baroclinic instability are met. In particular, at x=20 km (50 km) Π_x changes sign from positive (negative) in the upper 100 m to negative (positive) near 200 m.

The eddy density flux $\overline{u'\sigma'_\theta}$ calculated during times of the separated EGC dominant mode versus the NIJ dominant mode are shown in Figures 8a and 8b. One can see that the fluxes are significantly stronger in the latter scenario. In particular, a surface-intensified positive density flux is located 30-70 km offshore of the shelfbreak associated with isopycnals sloping upward toward shore, while a surface-intensified negative density flux appears in the inshore region with oppositely sloped isopycnals. The associated sections of baroclinic mean-to-eddy conversion reveal much larger values for the NIJ dominant state (compare Figures 8c and 8d; where positive values indicate that energy is being transferred from the mean to the eddies). There are two regions associated with high conversion: offshore near the edge of separated EGC, and onshore close to the front between the NIJ and the NIIC.

The eddy momentum flux $\overline{u'v'}$ calculated for the dominant separated EGC versus dominant NIJ periods are presented in Figures 8e and 8f. In the former case, the largest signal corresponds to a positive flux on the shoreward side of the separated EGC, associated with lateral shifts in the current. In particular, when the current moves offshore (onshore) it strengthens (weakens). In the latter case, the sign of eddy momentum flux changes from negative to positive going from west to east across the NIJ. This is associated with the fact that NIJ increases (decreases) in velocity when it moves seaward (shoreward). The sections of mean-to-eddy barotropic conversion are shown in Figures 8g and 8h. The primary conversion region is located near the front between the NIJ and NIIC, due to the large horizontal gradient of the along-stream velocity ($\frac{\partial \overline{v}}{\partial x}$).

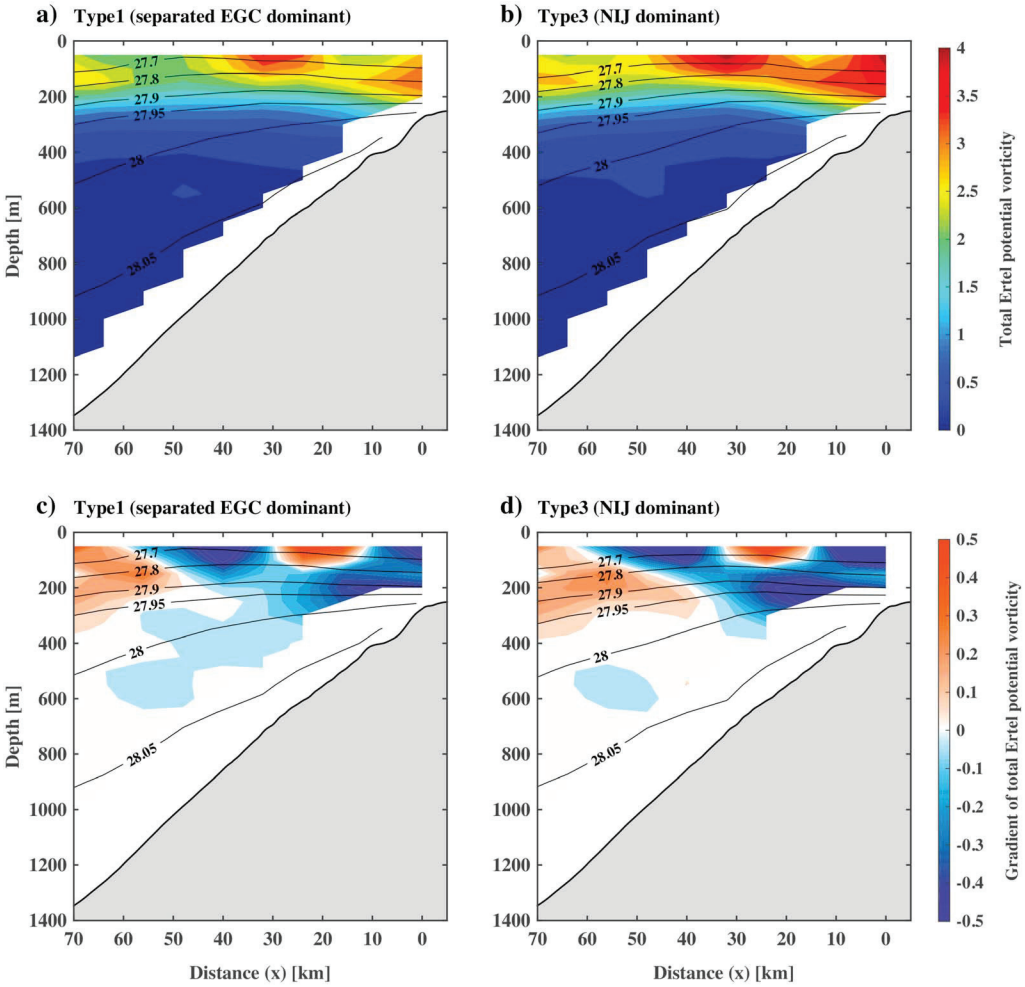

Figure 7. (a and b) Total Ertel potential vorticity [color, $10^{-10} \cdot m^{-1} \cdot s^{-1}$], and (c and d) the horizontal gradient of Ertel potential vorticity [color, $10^{-13} \cdot m^{-2} \cdot s^{-1}$] for the type1 and type3 configurations of the flow during the first year. The overlain contours are potential density [kg/m^3].

These results show that, generally, the baroclinic conversion from the mean to the eddies is much stronger than the barotropic conversion on the Iceland slope in the region of the Kögur array. Furthermore, it demonstrates that the baroclinic conversion in the region of the NIJ is significantly stronger when the NIJ is in its dominant state (the type3 scenario). The model simulation of Spall et al. (2019) also has a region of strong baroclinic eddy conversion north of Denmark Strait in the region of the NIIC hydrographic front, as we find here. They demonstrated that closer to the strait, this variability is coupled to the dense overflow water variability, which occurs throughout the year. Importantly, the baroclinic conversion shown here is present in all three configurations of the flow (types 1, 2, and 3), which is consistent with the fact that the instability at the Denmark Strait sill displays no seasonality. We have demonstrated, however, that when the NIJ is particularly strong the instability process is more effective.

3.4. Relationship Between the NIJ-Dominant Scenario and Upstream Atmospheric Forcing

We now seek to understand the difference in seasonal timing of the NIJ-dominant scenario in the two years of data, specifically to determine if it is related to the atmospheric forcing upstream of Denmark Strait. The atmospheric weather patterns in this region are dictated largely by the Icelandic Low and the topography of Greenland (e.g., Moore & Renfrew, 2005), as well as the Lofoten Low (Jahnke-Bornemann & Brümmer, 2009). The prevailing winds in Denmark Strait and the western Iceland Sea are out of the north. This is seen clearly in the two-year mean map of 10-m wind speed and sea level pressure (Figure 9a), where the mean is

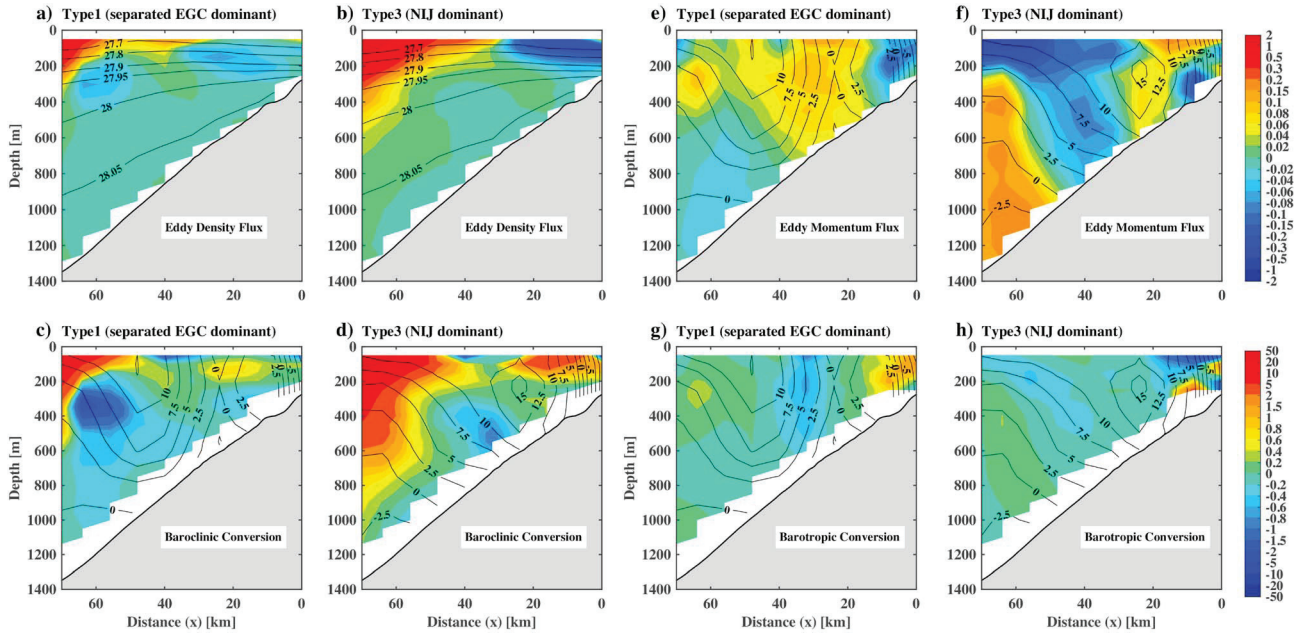

Figure 8. (a and b) Eddy density flux [color, 10^{-2} kg/m^2 s] and (c and d) mean-to-eddy baroclinic conversion term [color, 10^{-8} m^2/s^3] for the type1 and type3 configurations of the flow in year 1. (e and f) Eddy momentum flux [color, 10^{-2} m^2/s^2] and (g and h) mean-to-eddy barotropic conversion term [color, 10^{-8} m^2/s^3] for the type1 and type3 configurations of the flow in year 1. The overlain contours are potential density [kg/m^3] (a and b) and along-stream velocity [cm/s] (c-h).

taken over the cold months of the year (September to April). The Icelandic Low is evident in the southwest Irminger Sea, as is the effect of the Greenland barrier which helps channel the winds along the coast. The mean total turbulent heat flux (sensible + latent) is highest in a band extending from the northern Irminger Sea through Denmark Strait. While the mean fluxes in the western Iceland Sea (the boxed region in Figure 9, discussed below) are smaller, this region is governed by frequent cold-air outbreaks during winter which can result in strong fluxes for up to a week at a time (Harden et al., 2015; Moore et al., 2012).

There was a notable difference in the atmospheric forcing between the two study years (Figure 10). In particular, the Icelandic Low deepened from September through December in year 1; accordingly, the monthly wind in the vicinity of Denmark Strait was stronger from early-October to December (Figure 10a). In the

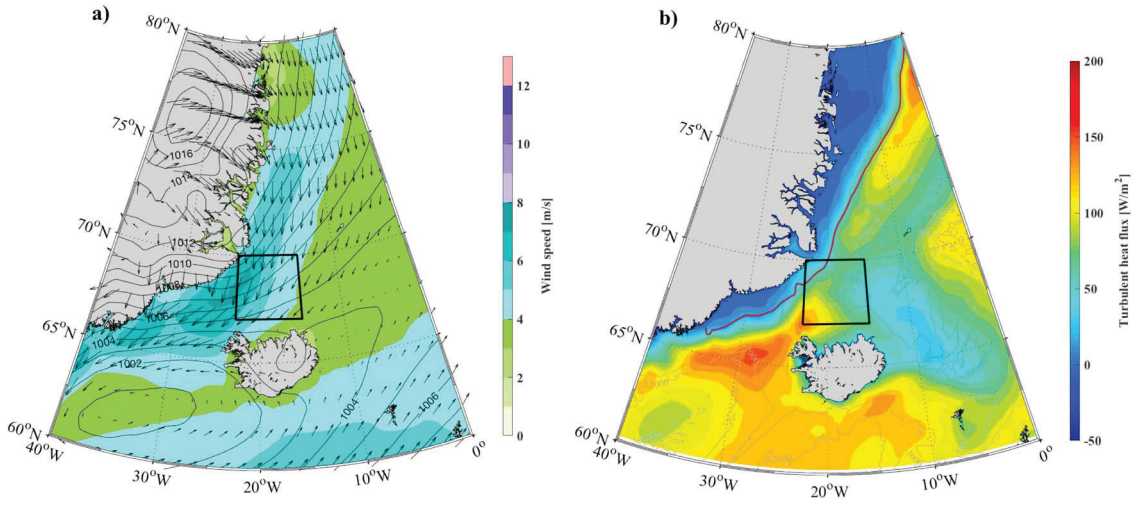

Figure 9. (a) Two-year mean wind field (2011–2013) for the months of September to April (color and vectors), overlain by the mean SLP (contours, mb). (b) Same as (a) except for the total turbulent heat flux (color). The dark red line represents the composite 50% sea ice concentration contour for winter months (December to February). The contours of bathymetry from ETOPO2 are shown in gray. The black box (15°-23° W, 67°-70° N) denotes the region used for calculating the spatially-averaged time series in Figure 10.

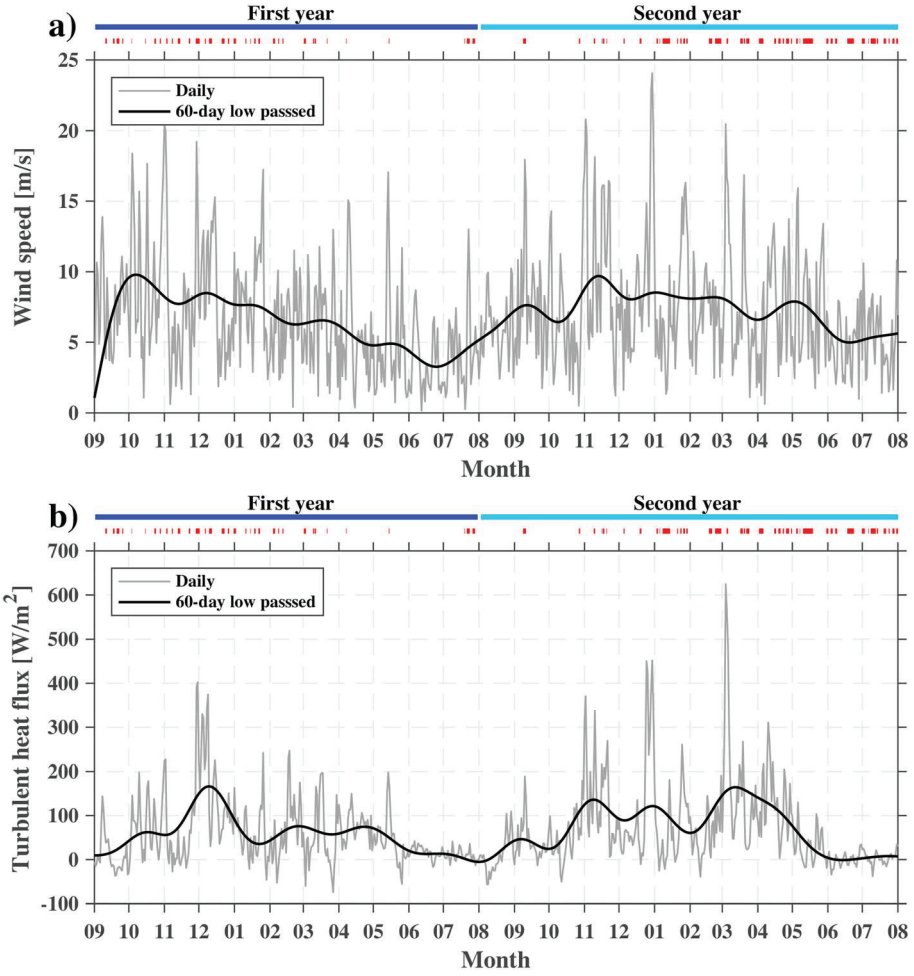

Figure 10. Time series of (a) daily (grey) and 60-day low-passed (black) wind speed and (b) turbulent heat flux from September 2011 to July 2013. The daily values of wind speed and turbulent heat flux are averaged within the boxed region of Figure 9 before using the low-pass filter. The horizontal lines on top of the panels indicate the time periods of mooring deployment in the first year (dark blue) and the second year (light blue), and the appearance of the type 3 configuration (red bars).

second year, the strong wind season shifted, starting in late-November and extending to April. A comparable change occurred with the monthly turbulent heat flux as well (Figure 10b). In particular, the oceanic heat loss reached its peak in December of the first year and in the March of second year. This interannual change in the timing of the strong atmospheric forcing, in light of the shift in phasing of the dominant NIJ

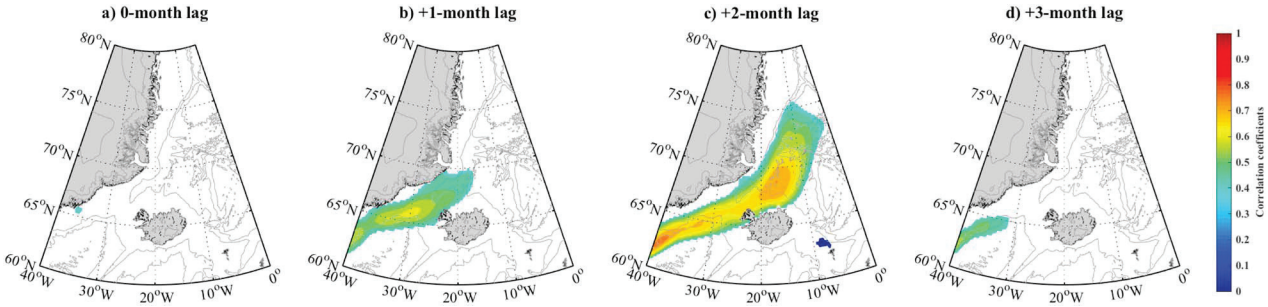

Figure 11. Spatial distribution of the lagged correlation between the monthly depth-mean along-stream velocity at the KGA4 mooring for the NIJ dominant mode, and the monthly wind speed at each grid point in the domain. The lag is listed above each panel. A positive correlation corresponds to the atmospheric signal leading the velocity at KGA4. Only regions with P values ≤ 0.05 in the Student's t-distribution test are shown.

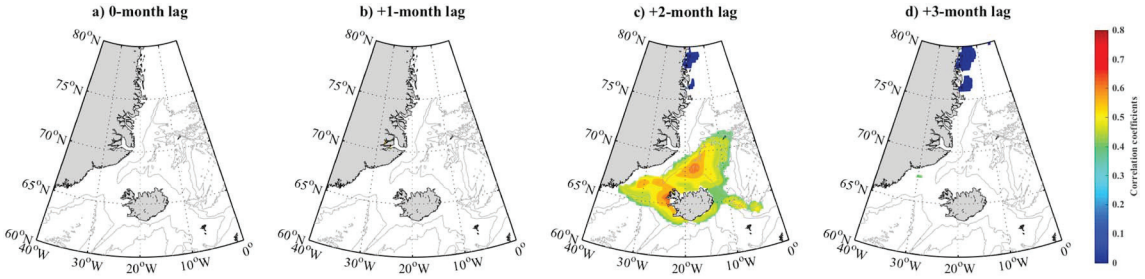

Figure 12. Same as Figure 11 except for the total turbulent heat flux.

occurrence between the two years discussed earlier (Figure 6), motivates consideration of possible links between the two.

To explore this, we correlated the time series of monthly velocity of the NIJ-dominant mode with the monthly wind speed and monthly total turbulent heat flux over a broad region centered on Denmark Strait, from September 2011 to July 2013. The results are shown in Figures 11 and 12. For both fields, there is a statistically significant region of correlation, passing the Student's *t* distribution test, with the largest values north of Iceland corresponding to a +2-month time lag (there were no correlations for negative time lags). The sense of the lag is such that the strong atmospheric forcing (i.e., higher winds and larger heat fluxes) leads the enhanced NIJ signature. We note that the same correlation pattern and lag arises for the latent heat and sensible heat fluxes individually (Figure 13).

What are the reasons for these correlations? We are unable to identify a causal relationship due to the wind stress alone, both for the region upstream or downstream of Denmark Strait. Specifically, the sense or the timing of coastal wave propagation is inconsistent with our observations (e.g., Allen, 1976). Furthermore, there is no significant correlation with regard to the regional wind stress curl. This implies that the buoyancy forcing is the primary reason for the correlations found here.

A physical explanation for the observed link between the turbulent heat flux and NIJ variability is provided by the study of Spall et al. (2017), who investigated the circulation response to an isolated region of dense water formation near an island. In their model, a region of deep convection was specified on the continental slope of the island over a relatively small geographical area. The resulting depression in sea surface height (SSH) excites Kelvin waves that propagate anticyclonically around the island. This in turn establishes a cyclonic circulation along the slope, which encircles the island due to the SSH gradient (lower height near the island). The wave response propagates at phase speeds in the range of 2-15 cm/s.

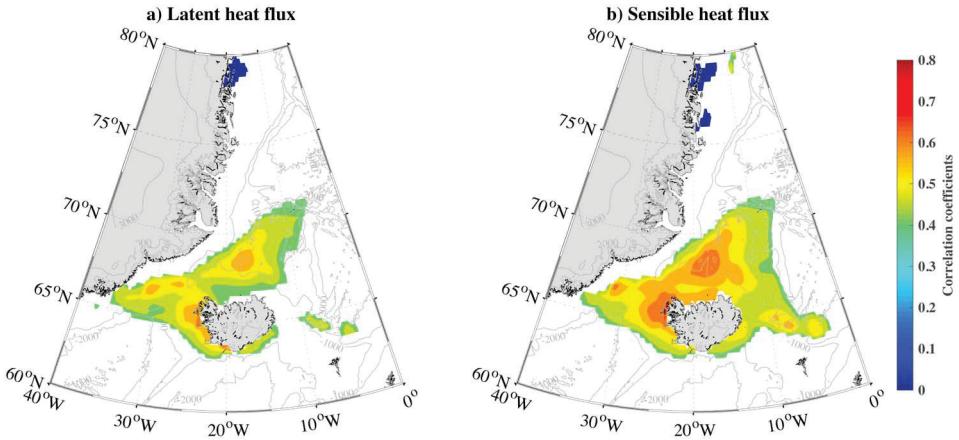

Figure 13. Spatial distribution of the +2-month lagged correlation between monthly depth-mean along-stream velocity at KGA4 mooring (Sep 2011 to Jul 2013) and (a) monthly latent heat flux and (b) monthly sensible heat flux, with *P* values ≤ 0.05 in the Student's *t*-distribution test.

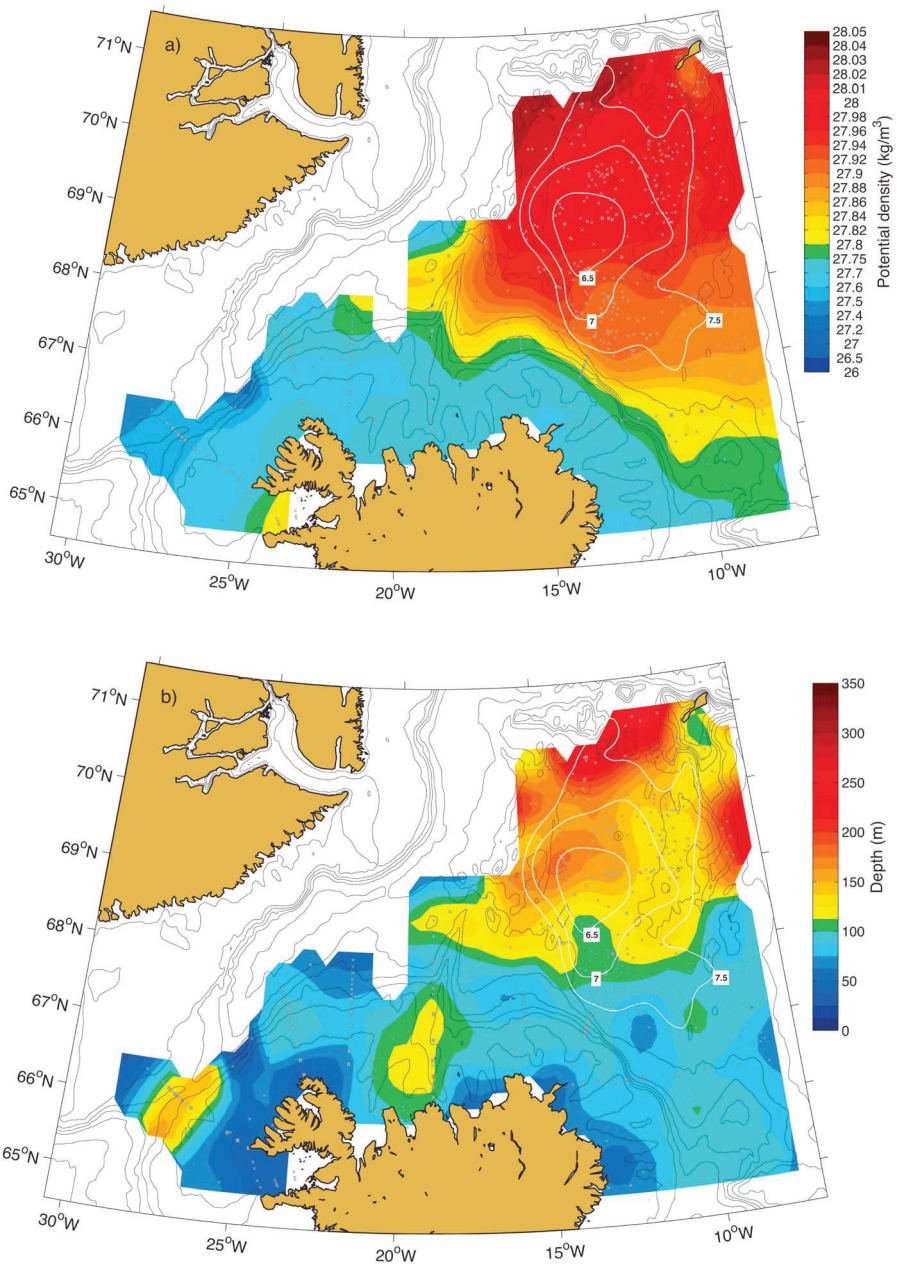

Figure 14. Distributions of late-winter mixed-layer properties in the Iceland Sea, from Våge et al. (2015). (a) Potential density [kg/m3], and (b) depth [m]. The white contours are dynamic height [dynamic cm] of the Iceland Sea Gyre relative to 500 db. The black lines are isobaths (200, 400, 600, 800, 1000, 1400, and 2000 m).

Close inspection of Figures 12 and 13 shows that the region of high correlation occurs on the north slope of Iceland, in the vicinity of the Kolbeinsey Ridge on the south side of the Spar Fracture zone (see Figure 1 for geographical names). A wave emanating from this location, propagating at the high end of the above range (15 cm/s), would reach the Kögur mooring array in roughly three months, resulting in the enhanced equatorward flow on the continental slope—that is, a stronger NIJ. This is of the correct order to explain the observed lag of two months (Figure 12).

There are two caveats to consider in this comparison. The first is that, in the model, the convection reaches the bottom, which is not the case in the observations. However, the response in the model is nearly barotropic (Spall et al., 2017) and should feel the bottom in the case of shallower convection. Furthermore, there

would be a sea surface depression regardless of the depth of convection. The second caveat is that there is no observational evidence to date for such a cyclonic circum-island flow. However, other factors could readily prohibit the signature of this, including the presence of Denmark Strait and hydraulic effects, wind forcing, and the subtropical-origin circulation in the vicinity of Iceland.

It is important to note we are not linking convection and dense water formation south of the Spar Fracture zone to the formation of the NIJ, but rather attempting to explain the monthly variability when the NIJ is in its dominant state. As noted in the introduction, it has been hypothesized that the source waters of the NIJ stem from the interior Iceland Sea (Våge et al., 2011). The deepest and densest wintertime mixed layers in the Iceland Sea are found farther to the north, at the outskirts of the Iceland Sea Gyre (Våge et al., 2015; see Figure 14). The air-sea forcing is also stronger in that area than near the Spar Fracture zone (Figure 9). It is thus more likely that the source waters of the NIJ emanate from the northwest Iceland Sea (or farther north). However, if the mechanism of Spall et al. (2017) is at work, the convection (and depression in SSH resulting from the convection) influencing the observed NIJ variability needs to take place on the Iceland continental slope.

Our results imply that there is only a small geographical area on the slope, south of the Spar Fracture Zone, where the sensitivity between the forcing and response is greatest (Figure 13). A likely reason for this is that the isobaths of the continental slope undergo a significant northward excursion there due to the Kolbeinsey Ridge (Figure 1). Våge et al. (2015) investigated the wintertime properties of the mixed layer in the Iceland Sea; Figure 14 shows their maps of climatological mixed-layer density and depth. One sees that the region in question corresponds to the deepest and densest mixed layers found anywhere on the continental slope north of Iceland. (We note that a winter cruise to the western Iceland Sea in February 2018 measured locally dense and deep mixed layers in this area.) Together, these results provide a dynamical explanation for the link found here between the atmospheric forcing and monthly variability of the NIJ.

4. Summary

Two years of mooring data from the Kögur section north of Denmark Strait were analyzed to better understand the structure and variability of the NIJ on the Iceland slope. Using the first year of data (September 2011 to July 2012), during which there were seven moorings deployed across the slope, three characteristic configurations of the flow were identified: (1) a strong separated EGC on the mid-Iceland slope and weak NIJ on the upper Iceland slope (referred to as type1), (2) a merged separated EGC and NIJ (type2), and (3) a strong NIJ located at its climatological mean position on the Iceland slope (roughly the 650-m isobath) and a weak signature of the separated EGC at the base of the Iceland slope (type3). The focus of the study was on type3, when the NIJ is dominant and advects anomalously dense water in its core.

The above classifications were identified by establishing a clear relationship between the different flow regimes and the depth-averaged flow at mooring KGA4 located at the canonical position of the NIJ. Since only KGA4 was deployed for the second year, this enabled us to parse out the three configurations of flow for that year as well (August 2012 to July 2013). We found that the NIJ dominant scenario was present during different times of the year for the two deployments—appearing mainly from September to February the first year, and from January to July the second year. Furthermore, when type3 was active it varied on short timescales characterized by the occurrence of pulses.

To understand the high-frequency variability of the NIJ dominant mode, we analyzed the Ertel potential vorticity and found that the cross-stream gradient of potential vorticity changes sign with depth, indicating baroclinic instability of the NIJ. To assess this further, we calculated the mean-to-eddy conversion for the three flow configurations using the first year of data. For type3 this revealed two high baroclinic conversion regions, one located near the edge of the separated EGC in the upper layer and the other one situated on the shoreward side of the NIJ at the front between the NIJ and the NIIC. The latter feature is consistent with recent model results suggesting that the NIJ upstream of Denmark Strait is intimately related to the high-frequency variability of dense overflow water at the Denmark Strait sill. Our results suggest that while the NIJ instability is present for the three flow configurations, it is enhanced for the dominant NIJ case.

To consider the seasonal timing of the NIJ dominant mode, we investigated the relationship between this state and the upstream atmospheric forcing. The time series of the monthly velocity of the NIJ dominant

type shows a significant 2-month lagged correlation with the monthly wind speed and turbulent heat flux in a localized region on the continental slope north of Iceland, with the atmospheric forcing leading the NIJ response. This region is south of the Spar Fracture zone, a gap in the Kolbeinsey Ridge, where the isobaths undergo an excursion to the north. Here the deepest and densest wintertime mixed layers are found along the continental slope north of Iceland (Våge et al., 2015). A dynamical explanation for the observed correlation lies in the context of Spall et al. (2017), who investigated the circulation response to a patch of dense water formation on the continental slope of an island. The Kelvin waves excited by the associated SSH depression set up a cyclonic circulation encircling the island. The timing of this process agrees well with the observed lagged response seen in our observations. While this can explain the monthly variability of the NIJ seen in the mooring data, it does not explain the origin of the current, which requires further investigation.

Acknowledgments
The authors thank the crew members of the R/V *Knorr*, RRS *James Clark Ross*, and R/V *Bjarni Sæmundsson* for the deployment and recovery of the moorings. D. Torres and F. Bahr processed the second year of mooring data. We thank K. Våge, B. Harden, Z. Song, J. Li, and M. Li for helpful discussions regarding the work. Funding was provided by the National Science Foundation under grants OCE-1558742 (J. H., R. P., P. L., and M. S.) and OCE-1534618 (M. S.). The mooring data are available at http://kogur.whoi.edu/php/index.php.

Reference

Allen, J. S. (1976). Some aspects of the forced wave response of stratified coastal regions. *Journal of Physical Oceanography*, *6*(1), 113–119. https://doi.org/10.1175/1520-0485(1976)006<0113:SAOTFW>2.0.CO;2

Behrens, E., Våge, K., Harden, B., Biastoch, A., & Böning, C. W. (2017). Composition and variability of the Denmark Strait Overflow Water in a high-resolution numerical model hindcast simulation. *Journal of Geophysical Research: Oceans*, *122*, 2830–2846. https://doi.org/10.1002/2016JC012158

Charney, J. G., & Stern, M. E. (1962). On the stability of internal baroclinic jets in a rotating atmosphere. *Journal of the Atmospheric Sciences*, *19*(2), 159–172. https://doi.org/10.1175/1520-0469(1962)019<0159:OTSOIB>2.0.CO;2

Dickson, R. R., & Brown, J. (1994). The production of North Atlantic Deep Water: Sources, rates, and pathways. *Journal of Geophysical Research*, *99*(C6), 12,319–12,341. https://doi.org/10.1029/94jc00530

Dukhovskoy, D. S., Myers, P. G., Platov, G., Timmermans, M. L., Curry, B., Proshutinsky, A., et al. (2016). Greenland freshwater pathways in the sub-Arctic Seas from model experiments with passive tracers. *Journal of Geophysical Research: Oceans*, *121*, 877–907. https://doi.org/10.1002/2015JC011290

Gierz, P., Lohmann, G., & Wei, W. (2015). Response of Atlantic overturning to future warming in a coupled atmosphere-ocean-ice sheet model. *Geophysical Research Letters*, *42*, 6811–6818. https://doi.org/10.1002/2015GL065276

Harden, B. E., & Pickart, R. S. (2018). High-frequency variability in the North Icelandic Jet. *Journal of Marine Research*, *76*(2), 47–62. https://doi.org/10.1357/002224018824845910

Harden, B. E., Renfrew, I. A., & Petersen, G. N. (2011). A climatology of wintertime barrier winds off southeast Greenland. *Journal of Climate*, *24*(17), 4701–4717. https://doi.org/10.1175/2011JCLI4113.1

Harden, B. E., Renfrew, I. A., & Petersen, G. N. (2015). Meteorological buoy observations from the central Iceland Sea. *Journal of Geophysical Research: Atmospheres*, *120*, 3199–3208. https://doi.org/10.1002/2014JD022584

Harden, R. S. P., Valdimarsson, H., Våge, K., de Steur, L., Richards, C., Bahr, F., et al. (2016). Upstream sources of the Denmark Strait Overflow: Observations from a high-resolution mooring array. *Deep Sea Research Part I: Oceanographic Research Papers*, *112*, 94–112.

Jahnke-Bornemann, A. N. N. I. K. A., & Brümmer, B. (2009). The Iceland–Lofotes pressure difference: different states of the North Atlantic low-pressure zone. *Tellus Series A: Dynamic Meteorology and Oceanography*, *61*(4), 466–475.

Jochumsen, K., Moritz, M., Nunes, N., Quadfasel, D., Larsen, K. M., Hansen, B., et al. (2017). Revised transport estimates of the Denmark Strait overflow. *Journal of Geophysical Research: Oceans*, *122*, 3434–3450. https://doi.org/10.1002/2017JC012803

Jochumsen, K., Quadfasel, D., Valdimarsson, H., & Jónsson, S. (2012). Variability of the Denmark Strait overflow: Moored time series from 1996–2011. *Journal of Geophysical Research*, *117*, C12003. https://doi.org/10.1029/2012JC008244

Jonsson, S., & Valdimarsson, H. (2004). A new path for the Denmark Strait overflow water from the Iceland Sea to Denmark Strait. *Geophysical Research Letters*, *31*, L03305. https://doi.org/10.1029/2003GL019214

Jónsson, S., & Valdimarsson, H. (2012). Hydrography and circulation over the southern part of the Kolbeinsey Ridge. *ICES Journal of Marine Science*, *69*(7), 1255–1262. https://doi.org/10.1093/icesjms/fss101

Käse, R. H., Serra, N., Köhl, A., & Stammer, D. (2009). Mechanisms for the variability of dense water pathways in the Nordic Seas. *Journal of Geophysical Research*, 114, C01013. https://doi.org/10.1029/2008JC004916

Köhl, A. (2010). Variable source regions of Denmark Strait and Faroe Bank Channel overflow waters. *Tellus A: Dynamic Meteorology and Oceanography*, *62*(4), 551–568. https://doi.org/10.1111/j.1600-0870.2010.00454.x

Köhl, A., Käse, R. H., Stammer, D., & Serra, N. (2007). Causes of changes in the Denmark Strait overflow. *Journal of Physical Oceanography*, *37*(6), 1678–1696. https://doi.org/10.1175/JPO3080.1

Mastropole, D., Pickart, R. S., Valdimarsson, H., Våge, K., Jochumsen, K., & Girton, J. (2017). On the hydrography of Denmark Strait. *Journal of Geophysical Research: Oceans*, *122*, 306–321. https://doi.org/10.1002/2016JC012007

Mauritzen, C. (1996). Production of dense overflow waters feeding the North Atlantic across the Greenland-Scotland Ridge. Part 1: Evidence for a revised circulation scheme. *Deep Sea Research Part I: Oceanographic Research Papers*, *43*(6), 769–806. https://doi.org/10.1016/0967-0637(96)00037-4

Moore, G. W. K., & Renfrew, I. A. (2005). Tip jets and barrier winds: A QuikSCAT climatology of high wind speed events around Greenland. *Journal of Climate*, *18*(18), 3713–3725. https://doi.org/10.1175/JCLI3455.1

Moore, G. W. K., Renfrew, I. A., & Pickart, R. S. (2012). Spatial distribution of air-sea heat fluxes over the sub-polar North Atlantic Ocean. *Geophysical Research Letters*, *39*, L18806. https://doi.org/10.1029/2012gl053097

Moore, G. W. K., Våge, K., Pickart, R. S., & Renfrew, I. A. (2015). Decreasing intensity of open-ocean convection in the Greenland and Iceland seas. *Nature Climate Change*, *5*(9), 877–882. https://doi.org/10.1038/nclimate2688

Pickart, R. S., Spall, M. A., Torres, D. J., Våge, K., Valdimarsson, H., Nobre, C., et al. (2017). The North Icelandic Jet and its relationship to the North Icelandic Irminger Current. *Journal of Marine Research*, *75*(5), 605–639. https://doi.org/10.1357/002224017822109505

Spall, M. A., Pedlosky, J., & Cenedese, C. (2017). Circulation induced by isolated dense water formation over closed topographic contours. *Journal of Physical Oceanography*, *47*(9), 2251–2265. https://doi.org/10.1175/JPO-D-17-0042.1

Spall, M. A., Pickart, R. S., Fratantoni, P. S., & Plueddemann, A. J. (2008). Western Arctic shelfbreak eddies: Formation and transport. *Journal of Physical Oceanography*, *38*(8), 1644–1668. https://doi.org/10.1175/2007JPO3829.1

Spall, M. A., Pickart, R. S., Lin, P., Valdimarsson, H., Haine, T. W. N., Alimansi, M., & Appen, W. (2019). Frontogenesis and variability in Denmark Strait and its impact on overflow water. *Journal of Physical Oceanography*. https://doi.org/10.1175/JPO-D-19-0053.1

Våge, K., Moore, G. W. K., Jónsson, S., & Valdimarsson, H. (2015). Water mass transformation in the Iceland Sea. *Deep Sea Research Part I: Oceanographic Research Papers*, *101*, 98–109. https://doi.org/10.1016/j.dsr.2015.04.001

Våge, K., Pickart, R. S., Spall, M. A., Moore, G., Valdimarsson, H., Torres, D. J., et al. (2013). Revised circulation scheme north of the Denmark Strait. *Deep Sea Research Part I: Oceanographic Research Papers*, *79*, 20–39. https://doi.org/10.1016/j.dsr.2013.05.007

Våge, K., Pickart, R. S., Spall, M. A., Valdimarsson, H., Jónsson, S., Torres, D. J., et al. (2011). Significant role of the North Icelandic Jet in the formation of Denmark Strait overflow water. *Nature Geoscience*, *4*(10), 723–727. https://doi.org/10.1038/ngeo1234